Protein Science (1998), 7:2156–2163. Cambridge University Press. Printed in the USA.

Structural characterization of the entire 1.3S subunit of transcarboxylase from *Propionibacterium shermanii*

D. VENKAT REDDY,[1] SVEN ROTHEMUND,[1] BHAMI C. SHENOY,[2] PAUL R. CAREY,[2] AND FRANK D. SÖNNICHSEN[1]

[1]Department of Physiology and Biophysics, Case Western Reserve University, Cleveland, Ohio 44106
[2]Department of Biochemistry, Case Western Reserve University, Cleveland, Ohio 44106

(RECEIVED March 16, 1998; ACCEPTED May 18, 1998)

Abstract

Transcarboxylase (TC) from *Propionibacterium shermanii*, a biotin-dependent enzyme, catalyzes the transfer of a carboxyl group from methylmalonyl-CoA to pyruvate in two partial reactions. Within the multisubunit enzyme complex, the 1.3S subunit functions as the carboxyl group carrier. The 1.3S is a 123-amino acid polypeptide (12.6 kDa), to which biotin is covalently attached at Lys 89. We have expressed 1.3S in *Escherichia coli* with uniform ^{15}N labeling. The backbone structure and dynamics of the protein have been characterized in aqueous solution by three-dimensional heteronuclear nuclear magnetic resonance (NMR) spectroscopy. The secondary structure elements in the protein were identified based on NOE information, secondary chemical shifts, homonuclear $^{3}J_{HNH\alpha}$ coupling constants, and amide proton exchange data. The protein contains a predominantly disordered N-terminal half, while the C-terminal half is folded into a compact domain comprising eight β-strands connected by short loops and turns. The topology of the C-terminal domain is consistent with the fold found in both carboxyl carrier and lipoyl domains, to which this domain has approximately 26–30% sequence similarity.

Keywords: biotin; carboxyl carrier protein; lipoyl domains; NMR

Transcarboxylase (TC) is a complex multisubunit biotin-dependent enzyme (1,200 kDa), composed of 30 polypeptide chains of three different subunits: the 12S subunit (360 kDa), the 5S subunit (120 kDa), and the 1.3S biotinyl subunit (12.6 kDa). In the intact form of TC, there are a total of six 12S monomers (60 kDa) in a cylindrical central unit, twelve 5S monomers (60 kDa) in six dimeric outer 5S subunits, and twelve 1.3S subunits (Wood, 1979; Wood & Kumar, 1985). The 1.3S subunit is the biotin carboxyl carrier unit with biotin covalently attached to the Lys 89 ϵ-amino group as a post-translational modification by holo-carboxylase synthetase (Shenoy & Wood, 1988).

TC's large size presently precludes direct structural studies at high resolution. However, the individual subunits can be obtained readily for study by disassociating the TC enzyme (Wood, 1979). The 1.3S subunit is particularly amenable for characterization by NMR spectroscopy due to its size, high-solubility, and the availability of an expression system. Further, this subunit is of interest because of its specific protein–protein interactions. It is recognized by the holocarboxylase synthetase in the cell, which adds the biotin prosthetic group post-translationally. In addition to 1.3S interacting directly with 12S and 5S to form the intact enzyme, 1.3S is also required at the 1.3S/5S (or 12S) interface for the transcarboxylation reactions to occur. The CO_2 moiety is only transferred when biotin is ligated to the 1.3S protein, biotin alone being unreactive (Shenoy et al., 1993a).

The C-terminal amino acid sequences of biotin carboxyl carrier protein domains (BCCP) are well conserved among different enzymes, implying the existence of a common protein fold for these proteins (Toh et al., 1993). Further, BCCPs in these regions are also similar in sequence and structure to lipoyl domains of lipoic acid-dependent enzymes. Three-dimensional structures have been reported for six lipoyl domains and one biotin carboxyl carrier protein. These include the lipoyl domains of *Bacillus stearothermophilus* pyruvate dehydrogenase complex (PDHC) (Dardel et al., 1993), a non-native hybrid lipoyl domain of *Escherichia coli* PDHC (Green et al., 1995), the N-terminal domain of *Azotobacter vinelandii* 2-oxoglutarate dehydrogenase complex (OGDHC) and pyruvate dehydrogenase complex (PDHC) (Berg et al., 1996; Berg et al., 1997), the lipoyl domain from the dihydrolipoyl succinyltransferase component of the 2-oxoglutarate dehydrogenase multienzyme complex (OGDHC) of *E. coli* (Ricaud et al., 1996), and

Reprint requests to: Frank D. Sönnichsen, Department of Physiology & Biophysics, School of Medicine, Case Western Reserve University, 10900 Euclid Avenue, Cleveland, Ohio 44106-4970; e-mail: frank@herring.phol.cwru.edu.

Abbreviations: BCCP, biotin carboxyl carrier protein; DSS, 4,4-dimethyl-4-silapentane-1-sulfonate; 1D, one-dimensional; 2D, two-dimensional; 3D, three-dimensional; HSQC, heteronuclear single-quantum coherence; NMR, nuclear magnetic resonance; NOE, nuclear Overhauser effect; NOESY, nuclear Overhauser enhancement spectroscopy; TOCSY, total correlation spectroscopy; TC, transcarboxylase.

the human inner lipoyl domain from the dihydrolipoylamide acetyltransferase subunit of pyruvate dehydrogenase complex (PDHC) (Howard et al., 1998). The three-dimensional structure of the C-terminal fragment of one biotin carboxyl carrier protein ($BCCP_{sc}$), of the *E. coli* acetyl-CoA carboxylase, has been characterized by X-ray crystallography (Athappilly & Hendrickson, 1995) and NMR spectroscopy (Yao et al., 1997). The folds of all proteins domain were shown to be quite similar, consisting of a compact, all-β domain comprising two four-stranded sheets.

In the present study, we report the first NMR-spectroscopic analysis of a complete carboxyl carrier protein. We assign the secondary structure, and characterize the fold of the 1.3S subunit of transcarboxylase. As expected from the 26–30% sequence identity (Athappilly & Hendrickson, 1995; Reddy et al., 1997) of 1.3S to other lipoyl domains and BCCPsc, we find that the C-terminal half of 1.3S folds into a similar compact β-sheet domain. The 50 residues at the N-terminus, however, are flexible and do not appear to form stable contacts to the folded C-terminal domain.

Results

Assignments

Two-dimensional ^{1}H-^{15}N HSQC spectra of the uniformly ^{15}N-labeled holo-1.3S subunit of transcarboxylase were recorded at various temperatures and pH values to identify optimal conditions for protein characterization. Based on signal intensity and line widths, the best data were obtained at 20 °C and pH 6.5. Figure 1A is representative of the data quality obtained and exhibits good chemical shift dispersion. For the 123 amino acid protein (with six prolines), 94 cross-peaks including some weak resonances were observed (other than side-chain resonances). For 23 residues no amide protons could be observed under these or any other experimental conditions.

Resonance assignments of the holo-1.3S transcarboxylase began with the assignment of CαH and CβH resonances from the HNHA and HNHB spectra, respectively. Spin systems of the various amino acids were then completed and identified by their characteristic patterns of cross-peaks in the 3D ^{1}H-^{15}N TOCSY-HSQC experiments. Complete TOCSY transfer was observed for 67 residues. Additionally, Asn and Gln residues were confirmed by their characteristic intraresidue NOEs between side-chain NH and CβH and CγH, respectively. Proline residues (58, 60, and 97) were identified using connectivities between their CδH and the CαH of the preceding residue in a 2D NOESY spectrum and/or the sequential connectivities between their CαH and the NH of the next residue in 3D ^{15}N NOESY spectra. The observation of these cross-peaks also indicated that the respective X-Pro peptide bonds are in *trans* conformation.

Sequence-specific backbone resonance assignments were obtained from a combination of 3D ^{1}H-^{15}N NOESY-HSQC and 3D ^{1}H-^{15}N TOCSY-HSQC spectra using standard procedures (Wüthrich, 1986). Typical NOEs such as NH(i − 1)-NH(i), CαH(i − 1)-NH(i), or CβH(i − 1)-NH(i) were identified and established sequential relationships. As an example, sequential connectivities between Val 82 and Ala 96 are highlighted in Figure 2. All residues from Ala 47 to the C-terminal Gly 123 could be sequentially assigned by this approach.

About 20 spin systems remained; of these, two spin systems were assigned to Arg 42 and Phe 31 due to their uniqueness in the remaining sequence. Further, 7 Gly, 4 Ala, 1 Thr, 1 Leu, 1 Ile residues were identified but could not be assigned sequentially due to overlap or lack of intensity in the NOESY experiments. However, these partial residue/spin-type assignments are consistent with the 1.3S sequence from residue Ile 29 to Ala 47, the latter being the beginning of the sequentially assigned C-terminal sequence. Additionally, four incomplete spin systems were observed.

Backbone flexibility

Steady-state ^{1}H-^{15}N NOEs (expressed as intensity ratios) were determined using ^{1}H-^{15}N NOE correlation spectra without and with ^{1}H saturation (Fig. 1B). Uncertainties in NOE ratios were estimated as standard deviations from duplicate measurements, and were found to average 2.6%. A total of 73 residues were characterized. Between residues 55 to 123, NOE ratios are similar for most of the residues (Fig. 3) and average to 0.7 ± 0.1. Starting at Gly 55, heteronuclear NOE ratios continuously decrease toward the N-terminus, and are increasingly negative for all cross-peaks assigned to residues preceding Lys 51. This observation unequivocally establishes the high structural flexibility of the N-terminal 50 residues of 1.3S and indicates that the reduced signal intensity or lack of cross-peak intensity in HSQC and related experiments (Fig. 1) is primarily due to fast amide exchange kinetics.

It should be noted that the biotin ureido NH protons were not observed in the ^{15}N-heteronuclear NMR experiments, as unlabeled biotin was added during the protein expression. Nevertheless, the side-chain amide of lysine (K89NHϵ in Fig. 1) to which the cofactor is covalently attached, was observed in all ^{1}H,^{15}N-HSQC–derived experiments and provides dynamic information of the prosthetic group. In the heteronuclear NOE experiment (Fig. 1B), K89NHϵ exhibited a negative NOE ratio, indicating that this side chain linking the biotin prosthetic group is very flexible. This observation is consistent with our previous conclusion that the biotin moiety in 1.3S does not interact with the protein-moiety (Reddy et al., 1997).

Secondary structure

On the basis of the heteronuclear NOE values, the C-terminal half of holo-1.3S (Gly 55 to Gly 123) appears to have a well-defined structure and stable fold in solution. This is confirmed by the measurement of amide proton exchange rates, which were obtained by monitoring the ^{1}H-^{15}N cross-peak intensity in 2D HSQC spectra at 25 °C and pH 6.0 as a function of time after dissolving the protein in D_2O. The exchange for all residues in the N-terminal, and for many residues in the folded C-terminal half of 1.3S was too rapid to be measured. However, 28 residues in the C-terminal half (between Gly 55 and Gly 123) exhibited a large protection against exchange (Fig. 4). After 4 days only six of these residues significantly exchanged, the remaining 22 residues still exhibited between 13 to 61% of their original signal intensity suggesting the presence of a very stable fold in the C-terminal domain.

Figure 4 summarizes all NMR observations such as sequential NOEs, amide proton exchange data, and CαH secondary chemical shifts for residues 50–123 of the holo-1.3S subunit. Also included are $^{3}J_{HNH\alpha}$ coupling constants for 60 residues, which could be determined from HA/HN intensity ratios in a 3D HNHA experiment (Vuister & Bax, 1993) due to the good dispersion of the ^{1}H-^{15}N correlations. The combined data clearly identify large areas of the β-structure. Eight β-strands were identified by the observation of strong sequential dαN NOEs, $^{3}J_{HNH\alpha}$ coupling con-

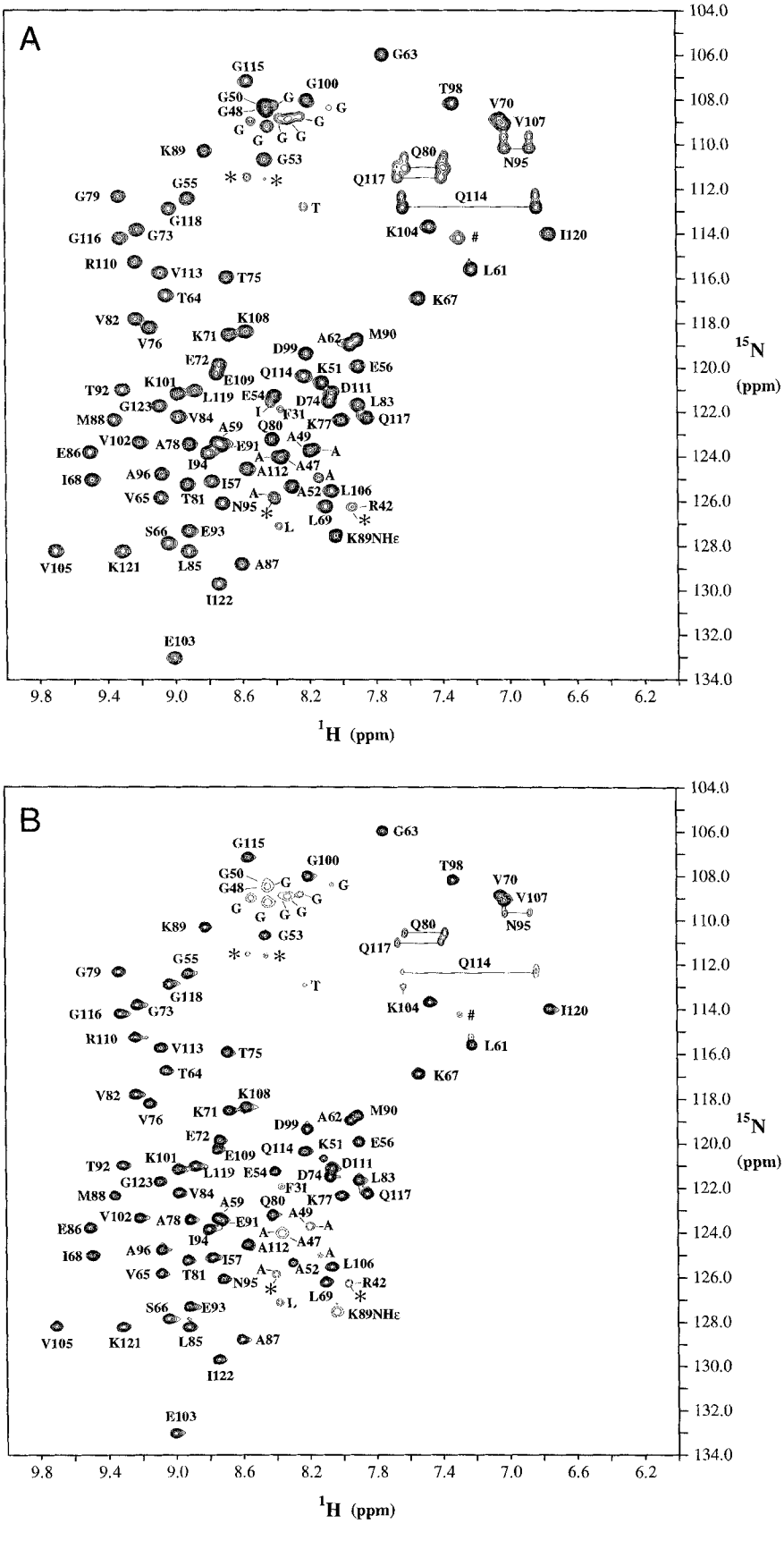

Fig. 1. Two-dimensional correlation spectra of uniformly ^{15}N-labeled holo-1.3S at pH 6.5 and 20 °C in 90% H_2O/10% D_2O (v/v). **A:** Contour plot of a ^{1}H-^{15}N HSQC spectrum. Cross-peaks are labeled with their amino acid type (one letter code) and sequence number. Side-chain amide resonances of Asn and Gln residues are connected by horizontal lines. Spin systems, which were identified by type but not assigned sequentially, are labeled without sequence number. Asterisks indicate residues that could not be identified and assigned due to overlap and/or low intensity of the cross-peak in the spectrum. The "#" symbol indicates a folded cross-peak corresponding to an Arg side chain. **B:** Contour plot of the ^{1}H-^{15}N heteronuclear NOE spectrum with pre-saturation. Negative cross-peaks are drawn with only two contours and dashed lines, and indicate residues that are showing negative NOEs.

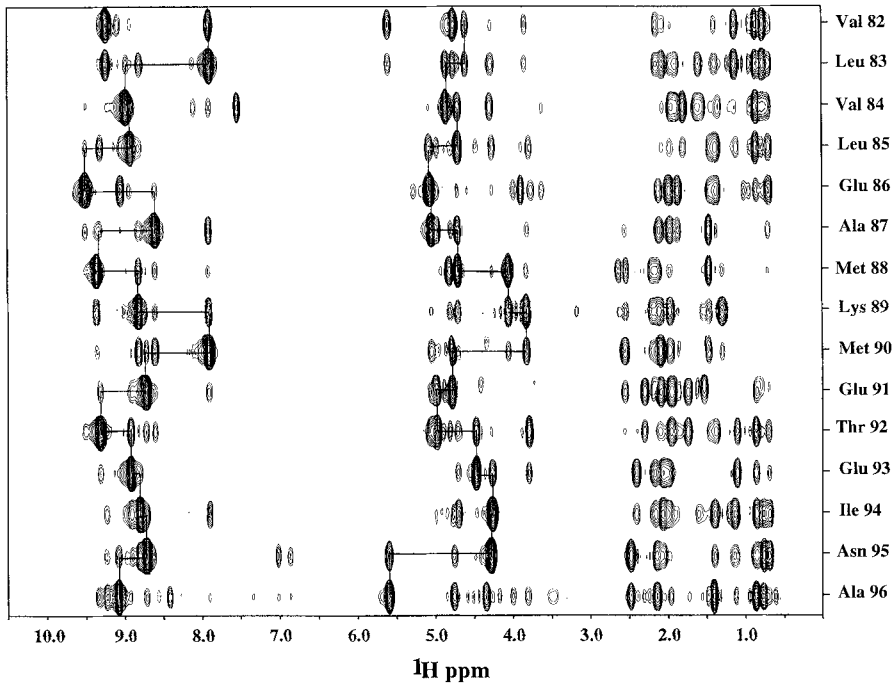

Fig. 2. Strip plot corresponding to amide planes for residues Val 82–Ala 96 taken from a 3D ^{1}H-^{15}N NOESY-HSQC spectrum of holo-1.3S. Sequential d_{NN} and $d\alpha$N NOE correlations are indicated by lines. The spectrum was recorded at 20 °C and pH 6.5 with a mixing time of 150 ms.

stants, CαH chemical shift data, the presence of slowly exchanging amide protons, and characteristic interstrand NOEs. Numbered consecutively from the N-terminus, β-strand I is rather short, as it includes only residues Glu 56 to Pro 58. The assignment is based on strong sequential $d\alpha$N (or equivalent $d\alpha\delta$) and downfield shifted CαH chemical shifts. Glu 56 and Ile 57, however, exhibit smaller $^3J_{HNH\alpha}$ coupling constants than expected, suggesting the presence of a less regular or more flexible β-strand. In β-strand II, which extends from Thr 64 to Leu 69, only three residues (Thr 64, Val 65, and Lys 67) exhibited protection against amide proton exchange indicating that this is an outer strand. The NOE pattern and small coupling constants in this strand suggest the presence of a β-bulge around Lys 67.

Applying primarily NOE, chemical shift, and coupling constant criteria, the regions from Thr 75 to Lys 77 and Val 82 to Glu 86 were assigned as strand III and IV, respectively. Almost all residues in these two strands showed large three bond HNHα coupling constants and positive CαH chemical shift differences. Although

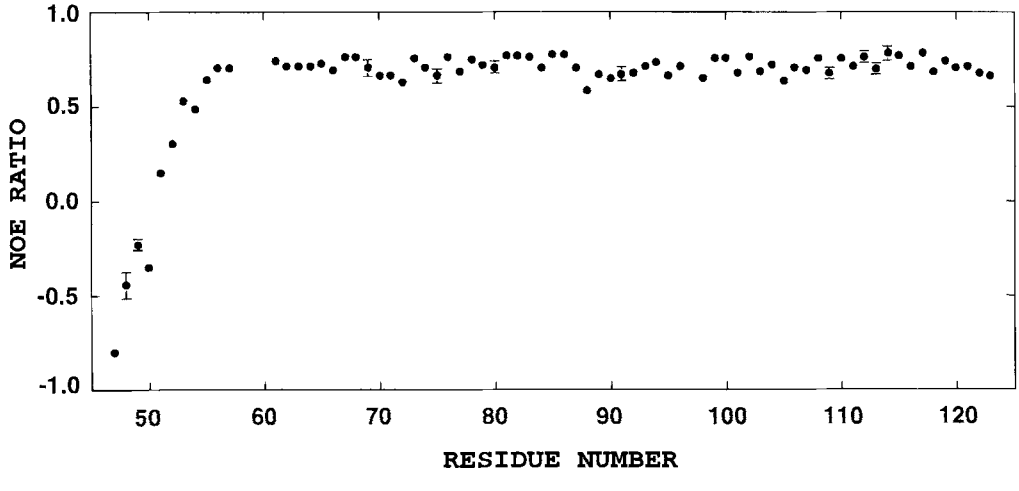

Fig. 3. Ratio of the steady-state ^{1}H-^{15}N heteronuclear NOEs with and without ^{1}H pre-saturation at 600 MHz for residues Ala47–Gly123 in holo-1.3S. Standard deviations in the measurements are indicated by error bars. For residues without error bars, the standard deviations are smaller than the symbol size.

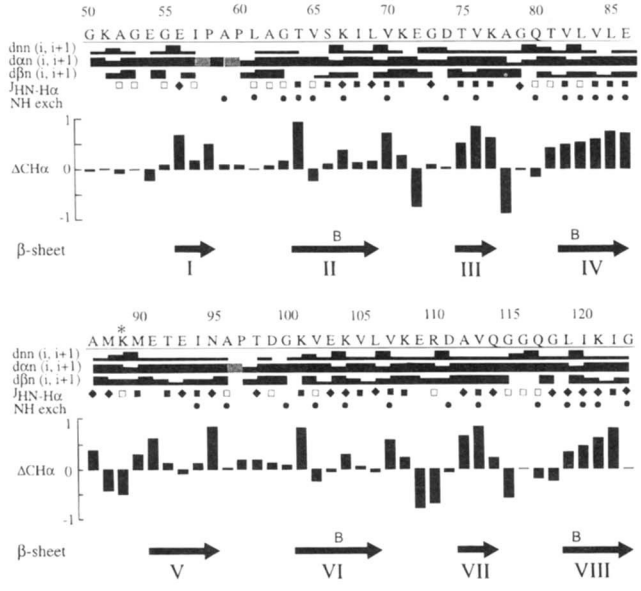

Fig. 4. Amino acid sequence and summary of the sequential NOEs, $^3J_{HNH\alpha}$ coupling constants, amide proton exchange data, and CαH secondary shifts obtained for residues 50–123 of holo-1.3S. NOEs: the height of the bars indicate the strength of the NOEs (strong, medium, and weak); a gray box denotes a sequential $d\alpha\delta$-NOE between a proline and its preceding residue. $^3J_{HNH\alpha}$ coupling constants were divided into three groups according to their magnitude: open square boxes, $J < 6$ Hz; diamonds, 6 Hz $< J >$ 8 Hz; and closed square boxes, $J >$ 8 Hz. Filled circles are used for residues with amide proton resonances that are not fully exchanged after 5 min. The location of β-strands identified from the data is shown in the bottom panel. The location of β-bulges is indicated by the letter "B" above the respective arrow, i.e., strand.

all amide proton resonances in strand IV show slow exchange, which is indicative of an inner strand in a β-sheet, only the amide proton of the middle residue in strand III (Val 76) did not exchange in D_2O. The presence of a strong d_{NN} connectivity between Val 82 and Leu 83 could indicate a β-bulge conformation in strand IV, similar to strand II.

β-Strand V extends from residues Glu 91 to Asn 95. All residues except Ile 94 exhibited rapid amide proton exchange indicative of a strand at the edge of a β-sheet. Strand VI (assigned from Lys 101–Leu 106) is a less regular strand, and its beginning is difficult to define, as several preceding residues exhibit small positive secondary chemical shifts as well as long-range NOE connectivities. Further, several J-values are smaller than expected, indicating that this strand is less regular when compared to most other strands. A β-bulge is implicated by the observation of strong d_{NN} between Glu 103 and Lys 104. Strands VII (Ala 112–Gly 114) and VIII (Leu 119–Gly 123) are clearly identifiable from their NOE patterns, supported primarily by large positive CαH secondary chemical shifts (up to 0.9 ppm) and continuous pathways of unambiguous strong $d_{\alpha N}$- and mostly weak d_{NN}- sequential NOEs. Four out of five residues in strand VIII were protected against amide proton exchange, indicative of a central strand. Small J-coupling values for several residues, and a strong d_{NN} between Leu 119 and Ile 120 suggest the presence of a β-bulge.

Residues Ala 59–Gly 63 between the β-strands I and II, and residues Ala 96–Gly 100 between strands V and VI form two small loops. Although they have some long-range interactions with strand VII and strand III (see below), they were not classified as regular β-strands due to very small CαH secondary chemical shifts and the absence of $^3J_{HNH\alpha}$ coupling constants of >8 Hz. Residues Lys 71–Asp 74 and residues Lys 77–Gln 80 appear to form two type II β-turns based on their NOE patterns (Wüthrich, 1986), creating a turn-strand-turn–like motif around strand III. Similarly, between strands VI and VIII, residues Glu 108–Asp 111, and residues Gln 114–Gln 117 form two type II β-turns completing another turn-strand-turn–like motif along with strand VII in the middle. Residues Ala 87–Met 90 are involved in a hairpin β-turn between strands IV and V, with the biotinyl residue located in the $(i + 2)$ position. This turn is recognized as a type I′ β-turn by its specific NOE pattern (Wüthrich, 1986).

β-Sheet topology

The eight strands observed in the 1.3S subunit of TC combine to form two β-sheets, each containing four β-strands of almost equal length arranged in an antiparallel fashion (Fig. 5). This topology was established on the basis of characteristic interstrand NH–NH, NH–CαH, CαH–CαH NOEs (Fig. 6A) and the analysis of the amide proton exchange data as described above. In particular, a large number of strong long-range CαH–CαH cross-peaks were observed in a 2D ^{1}H/^{1}H-NOESY experiment. These cross-peaks are indicative of characteristic short distances between CαH-protons remote in sequence, and are a distinctive feature of antiparallel β-strands.These characteristic cross-peaks are presented in a diagonal NOE plot (Fig. 6A). Off-diagonal peaks indicate the close spatial relationships of residues remote in sequence, primarily of residues in regions assigned as β-strands. The antiparallel nature of the sheets is exhibited by the cross-peak patterns running normal to the diagonal. Figure 6A further highlights one unusual property of the sheets. The fourth strand in each sheet (strands III or VII) has only limited contacts with its adjacent strand (strand VI or II, respectively), but displays several short distances to the loop preceding these strands (loop 5,6 and loop 1,2). This is schemat-

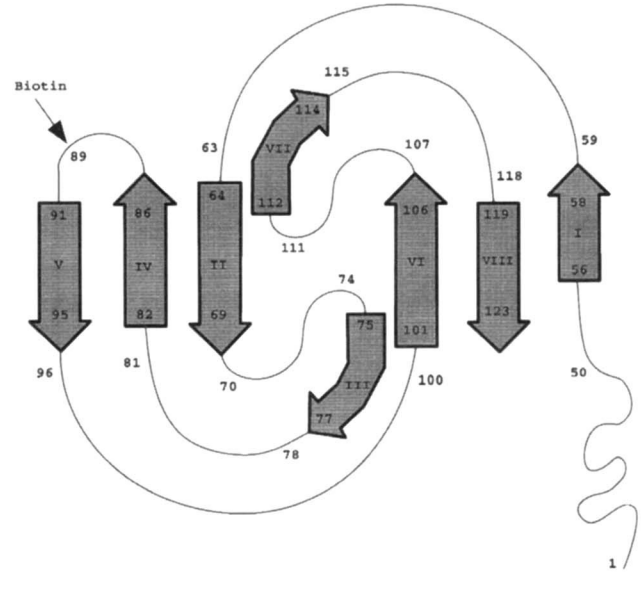

Fig. 5. Overall β-sheet topology for holo-1.3S as deduced from the NMR data. The residues involved in the corresponding β-strands are indicated with the residue number.

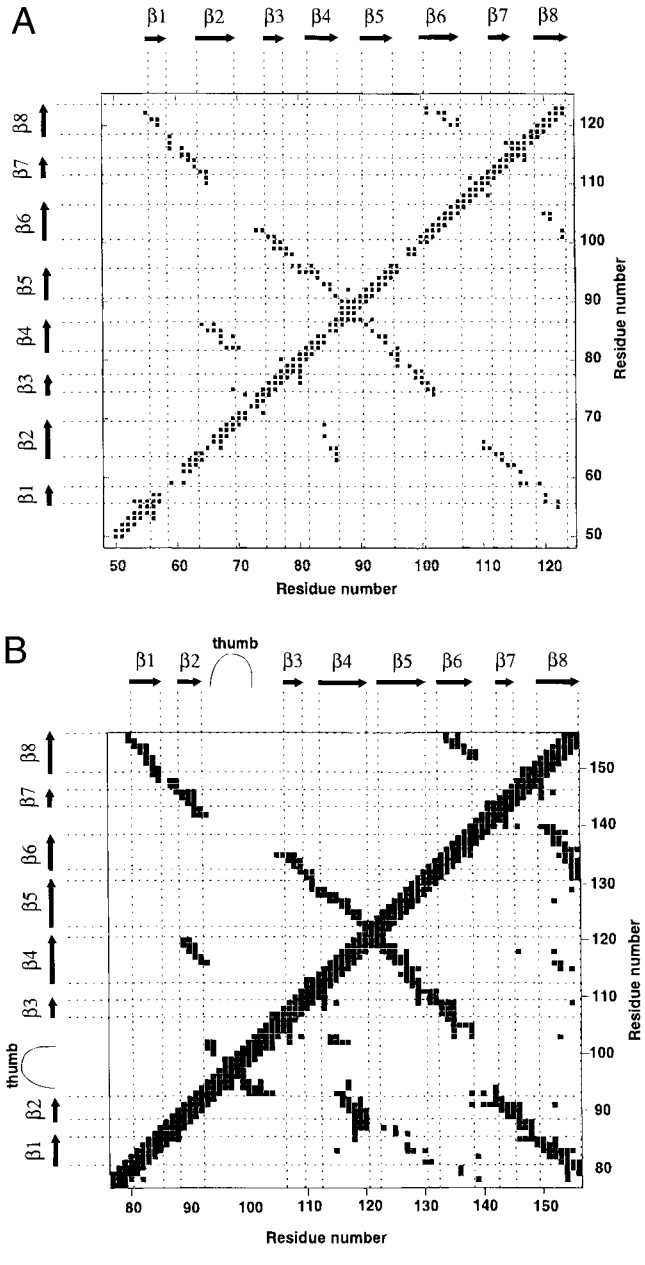

Fig. 6. Comparison of short-range distances in the C-terminal folded domains of 1.3S and BCCP. **A:** Off-diagonal squares indicate the presence of NOE cross-peaks between the respective residues in the NOESY experiments on 1.3S, indicative of distances <5 Å. Backbone-to-backbone NOE cross-peaks are shown below the diagonal, while side-chain backbone NOEs are shown above the diagonal. **B:** Diagonal plot of short-range distances in the crystal structure of BCCP (Athappilly & Hendrickson, 1995). The graph was generated with the program Molmol (Koradi et al., 1996).

ically illustrated in Figure 5 by the offset between the respective strands.

Discussion

In contrast to previous structural characterizations of biotin carboxylase carrier proteins, this investigation focuses on the entire biotin carboxyl carrier domain (1.3S) of transcarboxylase. Our study was facilitated by the good solubility of the 1.3S subunit near neutral pH values. The results show that 1.3S comprises two independent structural domains. The N-terminal domain ends close to Lys 51, and the C-terminal domain is comprised of residues Ala 52–Gly 123.

The N-terminal sequences in BCCP proteins leading up to the structured domain differ significantly in length and primary sequence (Samols et al., 1988; Athappilly & Hendrickson, 1995). In 1.3S, the sequence consists of approximately 50 residues that are essential for the protein's function (Kumar et al., 1982; Shenoy et al., 1993a). Residues 32 to 55 are very rich in Gly, Ala, and Pro residues, and are predicted to form a flexible loop or linker in the intact enzyme. This region before the folded domain of 1.3S is somewhat similar to the linker regions, which follow the lipoyl domains in the sequences of E2-chains of dehydrogenases (Perham, 1991; Berg & de Kok, 1997). The N-terminal 26 resides have been shown to be involved in specific protein–protein interactions with the other subunits to form the intact enzyme complex. In particular, residues 15–26 have been shown to bind to the outer subunits (5S), and residues 2–14 have been proposed to bind to the central subunits (12S) (Kumar et al., 1982). This sequence region contains an unusual $(DV)_3D$ motif, which has a high propensity to form an extended or β-conformation. Our data clearly show that the N-terminal domain is not interacting with the C-terminal domain of the 1.3S subunit (such as forming an additional strand with a sheet in the β-sandwich domain). It remains completely unstructured as indicated by the low intensity of most of its amide resonances due to chemical exchange, and most importantly, by the negative heteronuclear NOE values (Fig. 3). In future studies, it will be of interest to determine the structural changes in this domain, which are anticipated to occur upon interaction with the other subunits of the TC enzyme.

Residues 53 to 123 of 1.3S form a compact, folded domain. Two antiparallel sheets were identified, each comprised of four strands. Further, the topology (Fig. 5) is consistent with that observed for lipoyl domains (Ricaud et al., 1996; Berg & de Kok, 1997) and for the C-terminal fragment of BCCP of Acetyl-CoA carboxylase (Athappilly & Hendrickson, 1995), to which 1.3S has a sequence similarity of 30% in the entire folded domain. The structural model and NMR-spectroscopic data for 1.3S also agree with those of BCCP (Yao et al., 1997). Examples are the very similar β-strand locations and lengths, albeit some strand assignments here differ from those by Yao et al. (1997) by one or two residues. With one exception, all β-bulges are found in similar positions in strands IV, VI, and VIII. Moreover, in 1.3S several turns connecting the individual strands were identified as having identical turn-types as in BCCP. In particular, this was observed for the two turns around the short strands III and VII. These turn-strand-turn motifs, which run antiparallel to loops 1,2 and loop 5,6, were previously identified as unique structural motifs in BCCP and named "hammerhead" based on their appearance (Athappilly & Hendrickson, 1995). In 1.3S, we find evidence for a similar close spatial proximity between the second turn in the hammerhead motifs and the respective loops. A large number of NOEs (Fig. 6A), and several slowly exchanging amide protons within the loop regions (Ala 59, Leu 61 and Gly 63, Ala 96, and Gly 100) were observed (Fig. 4). Thus, it appears that the C-terminal domains of both BCCP and 1.3S have very similar tertiary structures.

A noteworthy property of the folded C-terminal domain (from residues 53 to 123) of 1.3S is its degree of symmetry. If one divides

this domain into two halves centered around the biotinyl residue 89 (as in Fig. 4, rows 1 and 2) these two halves exhibit nearly identical NMR properties. As an example, secondary chemical shifts, which are particularly sensitive to the local structural environment, are very similar almost through the entire two halves of the domain. Consequently, the secondary structure elements derived from these and the combined NMR data are nearly identical between these two regions. The only exception is β-strand I, which is two residues shorter than the equivalent strand V. Overall, the data suggest a very high twofold symmetry within the folded C-terminal domain.

The internal twofold symmetry has previously been noted for BCCP. A closer inspection of the NMR spectroscopic data between 1.3S and BCCP (Yao et al., 1997), however, indicates significant differences between these two protein domains. In BCCP, an internal comparison of secondary chemical shifts between the two halves of the characterized domain shows significant differences (Yao et al., 1997). This reflects structural differences between the two symmetry-related halves, and suggests that in BCCP the internal symmetry is lower than in 1.3S. The origin of this difference between the respective folds can, at this level, best be demonstrated by a comparison of the respective short-range distances observed for these two domains. Short range distance data for BCCP were derived from the crystal structure (Athappilly & Hendrickson, 1995), and for 1.3S from the observation of cross peaks in 2D and 3D NOESY experiments (Fig. 6A,B). In these figures, antiparallel strands are identifiable by rows of close distances between residues running normal to diagonal, establishing the close spatial relationships between the strands. Again, the high internal symmetry in 1.3S is obvious (Fig. 6A), as an exchange of the two halves (residues before residue 89 and residues after) would yield a nearly identical pattern. Such an exchange would not be possible for BCCP (Fig. 6B). Although in general a very similar pattern is observed, the symmetry is interrupted by an approximately seven-residue insertion between β-strands II and III. This region in BCCP has been named the protruding thumb (Athappilly & Hendrickson, 1995), but this thumb is absent in 1.3S.

As a consequence of the insertion of the "thumb" in the N-terminal half of BCCP, both halves of the 1.3S domain are more similar to the C-terminal half than to the N-terminal half of the BCCP domain. Secondary structure assignments as well as the secondary CαH chemical shifts are very similar between the C-terminal halves of these two domains, i.e., residues 89–123 in 1.3S and 122–156 in BCCP. Similarly, the NMR data of residues 54–88 in 1.3S show nearly identical secondary properties to residues 122–156 in BCCP. The same observation can be made on the sequence level, as a basic sequence alignment (Altschul et al., 1990) matches residues 56–86 of 1.3S with residues 126–156 of BCCP.

The lack of the protruding thumb in 1.3S is consistent with previous observations (Reddy et al., 1997). The characterization of the properties of the biotin moiety on 1.3S indicated that, in the absence of other subunits, the biotin is not interacting with the protein moiety of the 1.3S carrier domain. In contrast, the crystal structure of BCCP exhibited steric and hydrogen-bonding interactions between biotin and the protein involving a pocket formed between one antiparallel sheet and the protruding thumb. Yao et al. (1997) have suggested that for BCCP in solution similar biotin–protein interactions occur. The absence of such interactions in 1.3S can be explained given the absence of the thumb, which is responsible for the majority of protein–biotin interactions in BCCP (Athappilly & Hendrickson, 1995). Nevertheless, the role of the thumb and the significance of the presence or absence of protein–biotin interactions within the subunit for the mechanism of action remain undetermined.

In conclusion, the presented data characterize 1.3S as comprising of two domains. The C-terminal domain is folded and exhibits a compact β-sandwich structure nearly identical to BCCP and lipoyl domains. The domain is highly symmetric and lacks an extension called the "protruding thumb"in the BCCP protein. The N-terminal domain is found to be completely unstructured in solution, but it may be at least partially structured in the intact TC protein, as it encompasses the regions required for the proper enzyme assembly.

Materials and methods

Protein expression and purification

^{15}N-labeled 1.3S subunit was obtained by growing the overproducing strain of *E. coli* (CSH 26) containing ptac 1.3t plasmid in minimal medium at 37 °C with $^{15}NH_4Cl$ as the nitrogen source. The minimal medium contained 48 mM $Na_2HPO_4 \cdot 7H_2O$, 22 mM KH_2PO_4, 8.6 mM NaCl, 94 mM $^{15}NH_4Cl$, and 0.35 mM proline, 2 mM $MgSO_4$, 22 mM glucose, 0.1 mM $CaCl_2$, 0.5 mM biotin (unlabeled), and 0.03 mM thiamine. Protein production was induced using IPTG solution (0.4 mM final concentration) after the cells reached a density of 0.8 OD, and then continued to grow the cells for another 20 h before harvesting. The ^{15}N-labeled protein was then isolated as described previously for unlabeled 1.3S WT (Shenoy et al., 1993b).

NMR spectroscopy

NMR experiments were performed on a 2-mM holo-1.3S protein sample in 90% H_2O/10% D_2O (v/v). The sample pH was adjusted to 6.5 (not corrected for deuterium isotope effects) by addition of small volumes of DCl/NaOD, and DSS (0.1 mM) was added as an internal standard. Spectra were recorded on Varian UNITY Plus 600 MHz and INOVA 500 MHz spectrometers equipped with pulsed field gradient units and triple-resonance probes with an actively shielded z-gradients. The following experiments were recorded at 20 °C: 2D ^{1}H-^{15}N HSQC (Kay et al., 1992), ^{15}N-NOESYHSQC (Marion et al., 1989) spectra with a mixing time of 150 ms, ^{15}N-TOCSYHSQC (Zhang et al., 1994) spectra with various mixing times (30–60 ms), HNHA (Vuister & Bax, 1993), and HNHB experiments (Archer et al., 1991). All the heteronuclear experiments are improved pulsed field gradient, selectively enhanced experiments (Palmer et al., 1991) with water flip-back pulses for water suppression (Kay, 1995), with the exception of the HNHA experiment, which utilized jump and return water suppression. Typical carrier frequencies employed were 4.82 ppm for ^{1}H and 118.98 ppm for ^{15}N. ^{15}N decoupling was performed during acquisition with WALTZ-16 (Shaka et al., 1983). The data sets were processed using shifted sine-bell apodization and zero filling in both dimensions. Spectra were processed using the NMRPipe software system (Delaglio et al., 1995) and analyzed with the peak picking program PIPP (Garrett et al., 1991).

Amide-hydrogen exchange rates were determined by lyophilizing the protein from H_2O, dissolving the protein in D_2O. A series of 2D ^{1}H-^{15}N HSQC spectra at 25 °C and pH 6.0 were recorded on Varian INOVA 500 MHz spectrometer at intervals beginning 5 min

after the addition of D_2O, using 1,024 data points in F_1 and 160 complex increments in F_2 dimensions with eight scans per increment. Hydrogen exchange was followed for 4 days. A 2D NOESY spectrum was recorded at 20 °C and pH 6.5 in D_2O, with a collection of 2,048 data points in F_2 dimension, 256 complex data points in F_1 dimension with 16 scans per increment, and a mixing time of 100 ms. In order to remove the ^{15}N-^1H couplings a 180° refocusing pulse was used in the t_1 evolution period, and WALTZ-16 decoupling was applied during acquisition.

^1H-^{15}N steady-state NOE values were determined by HSQC-based pulse sequences (Farrow et al., 1994) at 20 and 25 °C. The spectra were recorded in the presence and absence of a ^1H saturation period of 3 s, with an overall relaxation delay of 5 s for both experiments, 1,024 data points in t_2 and 128 complex increments in t_1 with 16 scans per increment. All spectra were measured in duplicate, as well as at 600 and 500 MHz.

Acknowledgments

The present study was supported by a Research Initiation Grant of the Ohio Board of Regents (F.D.S.) and NIH Grant #DK53053 (P.R.C. and F.D.S.). The authors further thank Dr. L.E. Kay for making his pulse sequences available, and F. Delaglio and D. Garrett for their software packages NMRpipe and PIPP.

References

Altschul SF, Gish W, Miller W, Myers EW, Lipman DJ. 1990. Basic local alignment search tool. *J Mol Biol 215*:403–410.

Archer SJ, Ikura M, Torchia DA, Bax A. 1991. An alternative 3D NMR technique for correlating backbone ^{15}N with side chain Hb resonances in larger proteins. *J Magn Reson 95*:636–641.

Athappilly FK, Hendrickson WA. 1995. Structure of the biotinyl domain of acetyl-coenzyme A carboxylase determined by MAD phasing. *Structure 3*:1407–1419.

Berg A, de Kok A. 1997. 2-Oxo acid dehydrogenase multienzyme complexes. The central role of the lipoyl domain. *Biol Chem 378*:617–634.

Berg A, Vervoort J, de Kok A. 1996. Solution structure of the lipoyl domain of the 2-oxoglutarate dehydrogenase complex from *Azotobacter vinelandii*. *J Mol Biol 261*:432–442.

Berg A, Vervoort J, de Kok A. 1997. Three-dimensional structure in solution of the N-terminal lipoyl domain of the pyruvate dehydrogenase complex from *Azotobacter vinelandii*. *Eur J Biochem 244*:352–360.

Dardel F, Davis AL, Laue ED, Perham RN. 1993. Three-dimensional structure of the lipoyl domain from *Bacillus stearothermophilus* pyruvate dehydrogenase multienzyme complex. *J Mol Biol 229*:1037–1048.

Delaglio F, Grzesiek S, Vuister GW, Zhu G, Pfeifer J, Bax A. 1995. NMRPipe: A multidimensional spectral processing system based on UNIX pipes. *J Biomol NMR 6*:277–293.

Farrow NA, Zhang O, Forman-Kay JD, Kay LE. 1994. A heteronuclear correlation experiment for simultaneous determination of ^{15}N longitudinal decay and chemical exchange rates of systems in slow equilibrium. *J Biomol NMR 4*:727–734.

Garrett DS, Powers R, Gronenborn AM, Clore GM. 1991. A common sense approach to peak picking in two-, three-, and four-dimensional spectra using automatic computer analysis of contour diagrams. *J Magn Reson 95*:214–220.

Green JDF, Laue ED, Perham RN, Ali ST, Guest JR. 1995. Three-dimensional structure of lipoyl domain from the dihydrolipolyl acetyltransferase component of the pyruvate dehydrogenase multienzyme complex of *Escherichia coli*. *J Mol Biol 248*:328–343.

Howard MJ, Fuller C, Broadhurst RW, Perham RN, Tang JG, Quinn J, Diamond AG, Yeaman SJ. 1998. Three-dimensional structure of the major autoantigen in primary biliary cirrhosis. *Gastroentorology 115*:139–146.

Kay LE. 1995. Field gradient techniques in NMR spectroscopy. *Curr Opin Struct Biol 5*:674–681.

Kay LE, Keiffer P, Saarinen T. 1992. Pure absorption gradient enhanced heteronuclear single quantum correlation spectroscopy with improved sensitivity. *J Am Chem Soc 114*:10663–10665.

Koradi R, Billeter M, Wüthrich K. 1996. MOLMOL: A program for display and analysis of macromolecular structures. *J Mol Graphics 14*:51–55.

Kumar GK, Bahler CR, Wood HG, Merrifield RB. 1982. The amino acid sequences of the biotinyl subunit essential for the association of transcarboxylase. *J Biol Chem 257*:13828–13834.

Marion D, Driscoll PC, Kay LE, Wingfield PT, Bax A, Gronenborn AM, Clore GM. 1989. Overcoming the overlap problem in the assignment of ^1H NMR spectra of larger proteins by use of three-dimensional heteronuclear ^1H-^{15}N Hartmann-Hahn-multiple quantum coherence and nuclear Overhauser-multiple quantum coherence spectroscopy: Application to interleukin 1 beta. *Biochemistry 28*:6150–6156.

Palmer AG III, Rance M, Wright PE. 1991. Intramolecular motions of a zinc finger DNA-binding domain from Xfin characterized by proton-detected natural abundance ^{13}C heteronuclear NMR spectroscopy. *J Am Chem Soc 113*:4371–4380.

Perham RN. 1991. Domains, motifs, and linkers in 2-oxo acid dehydrogenase multienzyme complexes: A paradigm in the design of a multifunctional protein. *Biochemistry 30*:8501–8512.

Reddy DV, Shenoy BC, Carey PR, Sönnichsen FD. 1997. Absence of observable biotin–protein interactions in the 1.3S subunit of transcarboxylase: An NMR study. *Biochemistry 36*:14676–14682.

Ricaud PM, Howard MJ, Roberts EL, Broadhurst RW, Perham RN. 1996. Three-dimensional structure of the lipoyl domain from the dihydrolipoyl succinyltransferase component of the 2-oxoglutarate dehydrogenase multienzyme complex of *Escherichia coli*. *J Mol Biol 264*:179–190.

Samols D, Thornton CG, Murtif VL, Kumar GK, Hasse FC, Wood HG. 1988. Evolutionary conservation among biotin enzymes. *J Biol Chem 263*:6461–6464.

Shaka AJ, Keeler J, Frenkiel T, Freeman R. 1983. An improved sequence for broadband decoupling: WALTZ-16. *J Magn Reson 52*:335–338.

Shenoy BC, Kumar GK, Samols D. 1993a. Dissection of the biotinyl subunit of transcarboxylase into regions essential for activity and assembly. *J Biol Chem 268*:2232–2238.

Shenoy BC, Magner WJ, Phillips NFB, Kumar GK, Hasse FC, Samols D. 1993b. The nonbiotinylated form of the 1.3 S subunit of transcarboxylase binds to avidin (monomeric)-agarose: Purification and separation from the biotinylated 1.3 S subnit. *Protein Express Purificat 4*:85–94.

Shenoy BC, Wood HG. 1988. Purification and properties of the synthetase catalyzing the biotinylation of the apo subunit of transcarboxylase from *Propionibacterium shermanii*. *FASEB J 2*:2396–2401.

Toh H, Kondo H, Tanabe T. 1993. Molecular evolution of biotin-dependent carboxylases. *Eur J Biochem 215*:687–696.

Vuister GW, Bax A. 1993. A new approach for measuring homonuclear three-bond $J_{HNH\alpha}$ coupling constants in ^{15}N-enriched proteins. *J Am Chem Soc 115*:7772–7777.

Wood HG. 1979. The anatomy of transcarboxylase and the role of the subunits. *Crit Rev Biochem 7*:143–160.

Wood HG, Kumar GK. 1985. Transcarboxylase: Its quaternary structure and the role of the biotinyl subunit in the assembly of the enzyme and in catalysis. *Ann NY Acad Sci 447*:1–22.

Wüthrich K. 1986. *NMR of proteins and nucleic acids*. New York: J. Wiley and Sons.

Yao X, Wei D, Soden C Jr, Summers MF, Beckett D. 1997. Structure of the carboxy-terminal fragment of the apo-biotin carboxyl carrier subunit of *Escherichia coli* acetyl-CoA carboxylase. *Biochemistry 36*:15089–15100.

Zhang O, Kay LE, Olivier JP, Forman-Kay JD. 1994. Backbone ^1H and ^{15}N resonance assignments of the N-terminal SH3 domain of drk in folded and unfolded states using enhanced-sensitivity pulsed field gradient NMR techniques. *J Biomol NMR 4*:845–858.